



Mechanisms and model study of Zn(II) and Cd(II) competitive adsorption on V, Ti-bearing magnetite-humic acid adsorbent

Manman Lu, Yuanbo Zhang^{*,†}, Zijian Su^{*,†}, Shuo Liu, Jicheng Liu, Tao Jiang

School of Minerals Processing and Bioengineering, Central South University, Changsha, Hunan 410083, China, Tel. +86-13308498463; emails: sintering@csu.edu.cn/zybcsu@126.com (Y. Zhang), Tel. +86-15874285337; Fax: +86-731-88830542; email: szjcsu@163.com (Z. Su), Tel. +86-13278887816; emails: lmmcsu@163.com/lmm-csu@csu.edu.cn (M. Lu), Tel. +86-15827512265; email: lsus91@163.com (S. Liu), Tel. +86-18508431021; email: ljjcsu@126.com (J. Liu), Tel. +86-13808482537; email: jiangtao@csu.edu.cn (T. Jiang)

Received 14 September 2020; Accepted 27 February 2021

ABSTRACT

In this work, the adsorption characteristics and mechanisms of Zn(II) and Cd(II) on V, Ti-bearing magnetite-humic acid (VTM-HA) were deeply investigated. Several adsorption kinetics and isothermal models were introduced to describe the adsorption characteristics in single and binary ions systems. The results indicated that Zn(II) and Cd(II) adsorption both obey the pseudo-second-order kinetic model. Langmuir and extended Langmuir model could describe the adsorbing the details of single ion adsorption and binary ions competitive adsorption, respectively. The Zn(II) adsorption is dominant in the bi-component ion solution. Besides, the regenerative ability of the VTM-HA adsorbent is excellent. The adsorption capacity of Zn(II) and Cd(II) both remain more than 90% after five adsorption–desorption cycles. The Fourier transform infrared and X-ray photoelectron spectroscopy tests manifested that the hydroxyl and carboxyl groups of VTM-HA were the main active groups that participated in the adsorption reaction of Zn(II) and Cd(II). The density functional theory (DFT) calculation verified that Zn(II) ions have a more reliable combining ability with carboxyl and hydroxyl groups than Cd(II). That is why the Zn(II) has an advantage in competitive adsorption.

Keywords: Humic acid; Magnetic adsorbent; Zn(II) and Cd(II) ions; Adsorption; DFT calculation

1. Introduction

With the development of industry, the emissions of wastewater contained heavy metal has been an enormous menace to human health as well as all kinds of aquatic organisms [1,2]. Zn(II) and Cd(II) ions are severe environmental pollutants, which are the main toxic ingredients of industrial wastewater from mining, metallurgy, and chemical industry, etc. [3]. The environmental pollutions caused by Zn(II) and Cd(II) have been widely reported [4].

The adsorption process is the most generally used technology to treat heavy metals pollution because of its highly effective [5,6], economical and straightforward operation [7–9]. The recently published literature revealed that magnetic particles are the most widely used adsorbents due to the easy recycling by magnetic separation [10,11]. Aim to improve the adsorption capacity of the magnetic adsorbent and enhance the adsorption efficiency. Some novel adsorbents are developed by coating the organic matters on the surface of the magnetic adsorbent [12–14]. However,

* Corresponding author.

†These authors have contributed equally to this work

the most researched magnetic adsorbents are Fe_3O_4 and MFe_2O_4 ($\text{M} = \text{Co}, \text{Mn}, \text{Ni}, \text{Zn}, \text{Ca}, \text{etc.}$) spinel nano-particles [15]. These nano-particles are mostly prepared using the hydration synthesis method or co-precipitation method, which has many disadvantages such as difficulty in preparation, high cost, and low production efficiency [16]. These deficiencies limit the large-scale industrial application of these nano-adsorbents. Based on the above reasons, some researchers had paid their attention to the natural magnetic minerals [17]. A number of studies had verified that some natural minerals have an excellent adsorption capacity for heavy metal ions after fine grinding and surface modification [18]. The V, Ti-bearing magnetite-humic acid (VTM-HA) is a novel magnetic adsorbent developed by the authors' group [19]. The VTM-HA adsorbent is prepared by modifying natural V, Ti-bearing magnetite (VTM) particles with humic acid (HA) coating. The VTM is formed by replacing some Fe atoms in ordinary magnetite with Ti and V atoms. The Fe_3O_4 and Fe_2TiO_4 in the VTM make VTM-HA adsorbent have good magnetism and easy to be recovered by magnetic separation. What is more, our previous research had verified that the Ti atoms in VTM have a stronger adsorption capacity for HA compared to the Fe atoms in the ordinary magnetite (Fe_3O_4) [20]. Therefore, more HA could be adsorbed on the VTM surface, thereby providing more adsorption sites for Zn(II) and Cd(II). Humic substance is a kind of natural organic matter (NOM) [21]. Much literature verified that there is strong complexation between oxygen-bearing functional groups of HA, especially hydroxyl and carboxyl groups and metal cations on mineral surfaces [22–24].

Many published studies had reported that when in an aqueous system with several kinds of heavy metal ions, there is competitive adsorption between different heavy metal ions [25–27]. Fan et al. [28] prepared an adsorbent, tetraethylenepentamine (TEPA) modified chitosan/ CoFe_2O_4 particles for the removal of Pb(II) and Cu(II). This research indicated that the TEPA modified chitosan/ CoFe_2O_4 adsorbent showed high magnetization and efficient adsorption performance on Pb(II) and Cu(II), the adsorption experiments manifesting that maximum adsorption capacity of Pb(II) and Cu(II) in the binary system were less than that in the single system. This was because the active adsorbing sites on the adsorbent surface are limited. There was competition adsorption between Cu(II) and Pb(II) ions. An earlier article compared the binding ability of Cu(II), Cd(II), and Pb(II) with pure HA by adopting a modeling method. Among these three metal ions, the sequence of binding strength with HA was $\text{Pb(II)} > \text{Cu(II)} > \text{Cd(II)}$ [29]. Numerous researchers have researched the interaction between metal ions and HA [30,31]. In the past years, most studies deemed carboxylic and hydroxy as the essential functional adsorption sites for heavy metal ions, and each heavy metal ion has its specific adsorption site [32,33]. However, there was a lack of a comprehensive experimental study and detailed discussions about heavy metals adsorption onto pure HA or HA composite adsorbents in the published literature.

The highlights of this study were to contrast the adsorption characteristics of the Zn(II) and Cd(II) on the VTM-HA adsorbent in single and binary ions systems and introduce three models to describe the competitive

adsorption characteristics. Also, the regenerating ability of the VTM-HA adsorbent was verified by adsorption-desorption experiments. The Fourier transform infrared (FTIR), X-ray photoelectron spectroscopy (XPS) analyses, and density-functional theory (DFT) calculations were performed to explore the reasons for the differences between these two ions in competitive adsorption.

2. Materials and methods

2.1. Materials

The novel adsorbent named VTM-HA was produced via modifying the original VTM particles. The naked VTM particles were firstly ground to nano-size ($d_{0.5} = 201 \text{ nm}$, specific surface area = $104.99 \text{ m}^2/\text{g}$). Subsequently, the nano-VTM particles were added into the HA solution and stirred to prepare the VTM-HA adsorbent. The VTM-HA adsorbent preparation details were described in the previous paper of the authors' group [19]. In this research, the simulated heavy metal ions solutions were used to replace real wastewater. The simulated heavy metal ion-containing solutions were prepared from ZnCl_2 and CdCl_2 .

2.2. Adsorption experiments

In each experiment, 50 mL Zn(II) and Cd(II)-containing solution was used and added into an Erlenmeyer flask. Then, 20 mg of VTM-HA adsorbent was added into the simulated heavy metal ions solution. 0.1 mol/L NaOH and HCl solutions were used to adjust the pH value of the Zn(II) and Cd(II)-containing solution. The initial pH values changed from 3 to 8. Finally, the mixed liquors under different experimental conditions were oscillated for 24 h at 298 K to achieve adsorption equilibrium. After oscillating, the suspensions were subjected to a solid-liquid separation operation by a centrifuge. The obtained supernatants were analyzed by inductively coupled plasma mass spectrometry (ICP-MS) technology. The results were considered as Zn(II)/Cd(II) concentration after adsorption.

The adsorption kinetics study was performed under various contact times. The contact time was designed from 10 to 1,440 min. The initial metal ions concentrations and pH values of Zn(II) and Cd(II) solutions were controlled at 10 mg/L and 7, respectively. The Erlenmeyer flasks oscillated at 298 K.

The adsorption equilibrium fitting experiments were carried out under different initial concentrations of Zn(II) and Cd(II) from 5 to 40 mg/L. The adsorption equilibrium fitting experiments were both conducted in single and binary metal ions solution. The temperature and pH value of Zn(II) and Cd(II)-containing solutions were kept at 298 K and 7, respectively.

In binary adsorption experiments, the Zn(II)/Cd(II) binary solution was used to conduct the adsorption equilibrium fitting experiments. The concentration ratio of Zn(II) and Cd(II) was variable depends on the experimental conditions. In this study, the concentration ratio of target ion and competing ion was set at 1:0.5, 1:1, and 1:2 in order to investigate the effects of competing ion concentration changes on the adsorption of target ion. When Zn(II)

was considered the target ion, the Zn(II) concentration was controlled from 5 to 40 mg/L. The competing ion Cd(II) concentration was set at 2.5–20, 5–40, and 10–80 mg/L, respectively, and vice versa.

The amount of Zn(II) and Cd(II) adsorbed on VTM-HA adsorbent was suggested to be calculated by the following equation:

$$q_e = \frac{(C_0 - C_e)V}{m} \quad (1)$$

where q_e is the amount of Zn(II) and Cd(II) adsorbed on VTM-HA adsorbent (mg/g); C_0 and C_e are the initial and equilibrium concentrations of Zn(II) and Cd(II) (mg/L), respectively; V is the volume of Zn(II) and Cd(II) simulated solution (L); m is the VTM-HA adsorbent mass (g).

2.3. Characterization

High-resolution transmission electron microscopy (HRTEM) was conducted using a JEOL 2100 F transmission electron microscopy (TEM) at an accelerating voltage of 200 kV. The FTIR analysis was performed using a FTIR spectrometer (USA Thermo Nicolet Nexus 670 FTIR spectrometer). 1 mg samples were blended with 100 mg IR-grade KBr powder and then analyzed. A wide range of 500–4,000 cm^{-1} was adopted in FTIR analysis. The hysteresis loops were measured using a vibrating sample magnetometer (LDJ 9600, USA).

The binding energy of the atomic orbital of VTM-HA adsorbents before and after adsorbing Zn(II)/Cd(II) was studied through XPS analysis. The XPS testing condition in this research is Mono 650 μm , 200 W, Al $K\alpha$, and pass energy 20 eV. The energy step of full-scanning spectra is 1.0 eV, while the energy step of high-resolution scanning is 0.1 eV.

Considering the heterogeneity of HA molecular, two basic active functional groups involved in the Zn(II)/Cd(II) adsorption, acetic acid, and ethyl alcohol were chosen to carry out DFT calculation. The DFT calculations were conducted with Gaussian 09 package. The 6–311 ++ G (d, p) and LANL2DZ basis sets were adopted for DFT calculations at the B3LYP level [34].

3. Results and discussion

3.1. Characterization of VTM-HA adsorbent

The VTM-HA adsorbent is constituted basically by natural V, Ti-bearing magnetite and humic acid. The surface area and total pore volume for VTM and VTM-HA were 117.84 m^2/g , 0.398 cm^3/g , and 92.57 m^2/g , 0.2809 cm^3/g , respectively. It could be seen that the surface area and total pore volume for VTM-HA were both lower than those of VTM. This was because the HA existed on the VTM surface, covering some cracks of VTM particles.

The FTIR spectra of VTM displayed in Fig. 1 show that the FTIR peaks of VTM mainly belonged to the two ingredients, inorganic iron oxide and adsorbed water. The typical broad and intense band centered at 3,401 cm^{-1} was attributed to the associated O–H stretching vibrations. The peaks at 1,639 and 1,523 cm^{-1} were generally considered as the sign

of the O–H adsorption peak. These peaks of hydroxyl were produced by the water adsorbed on the VTM surface [35]. On the other hand, the peak at 913 cm^{-1} was derived from the hydroxylation of the VTM surface. This result manifested that the VTM surface contains abundant adsorption sites for HA. The peaks at 573 and 433 cm^{-1} were generally considered to belong to the Fe–O and Ti–O bonds of VTM [36,37]. After adsorbing HA, the peaks of hydroxylation, Fe–O and Ti–O bonds did not change, indicating that the adsorption of HA could not influence the surface structure of VTM. Besides, two new peaks at 1,544 and 1,384 cm^{-1} attached to the COO– group emerged [38]. It was obvious evidence which suggested that there are some complexation reactions between HA and VTM particles.

The TEM images displayed in Fig. 2 indicate that the HA adsorption reduced the agglomeration degree of VTM particles. The primary reason is that the strong electronegativity of HA adsorbed on the VTM surface, enhancing the electrostatic repulsion between VTM-HA particles. The excellent dispersion of VTM-HA adsorbent is conducive for adsorbing the Zn(II) and Cd(II) ions.

As a magnetic adsorbent, the magnetic property of VTM-HA is essential for magnetic separation recovery. Fig. 3 illustrates the hysteresis loops in the field cycling between ± 30 KOe. The magnetization curves for the VTM and VTM-HA showed hysteresis with good symmetry and weak magnetization. The saturation magnetization (M_s) values of VTM and VTM-HA were 23.61 and 21.42 emu/g , respectively. The magnetization of VTM-HA was slightly lower than the VTM possibly due to the presence of the HA layer. Some studies indicated that the carbon-based material could be a diamagnetic material over the magnetic phase attenuating saturation of magnetization [39]. The hysteresis of the VTM and VTM-HA revealed small coercivities at about 102 Oe. This result showed that the VTM-HA adsorbent could be classified as a superparamagnetic nanomaterial. The narrow hysteresis manifested that the VTM-HA is easy to magnetize and showed low coercivity. The above magnetic properties analyses reflected that

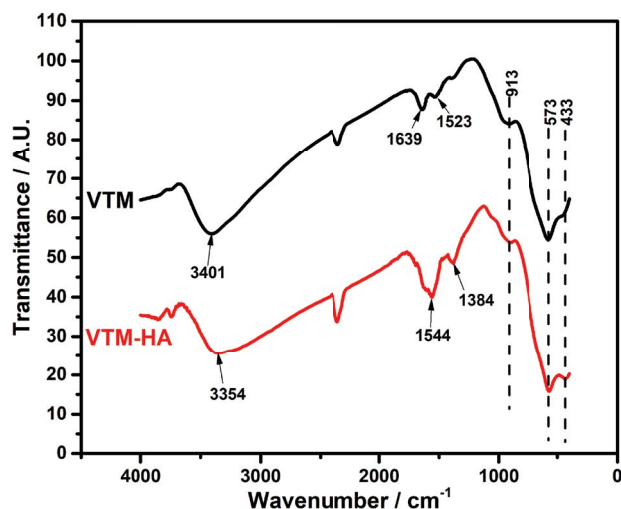


Fig. 1. FTIR spectra of VTM and VTM-HA.

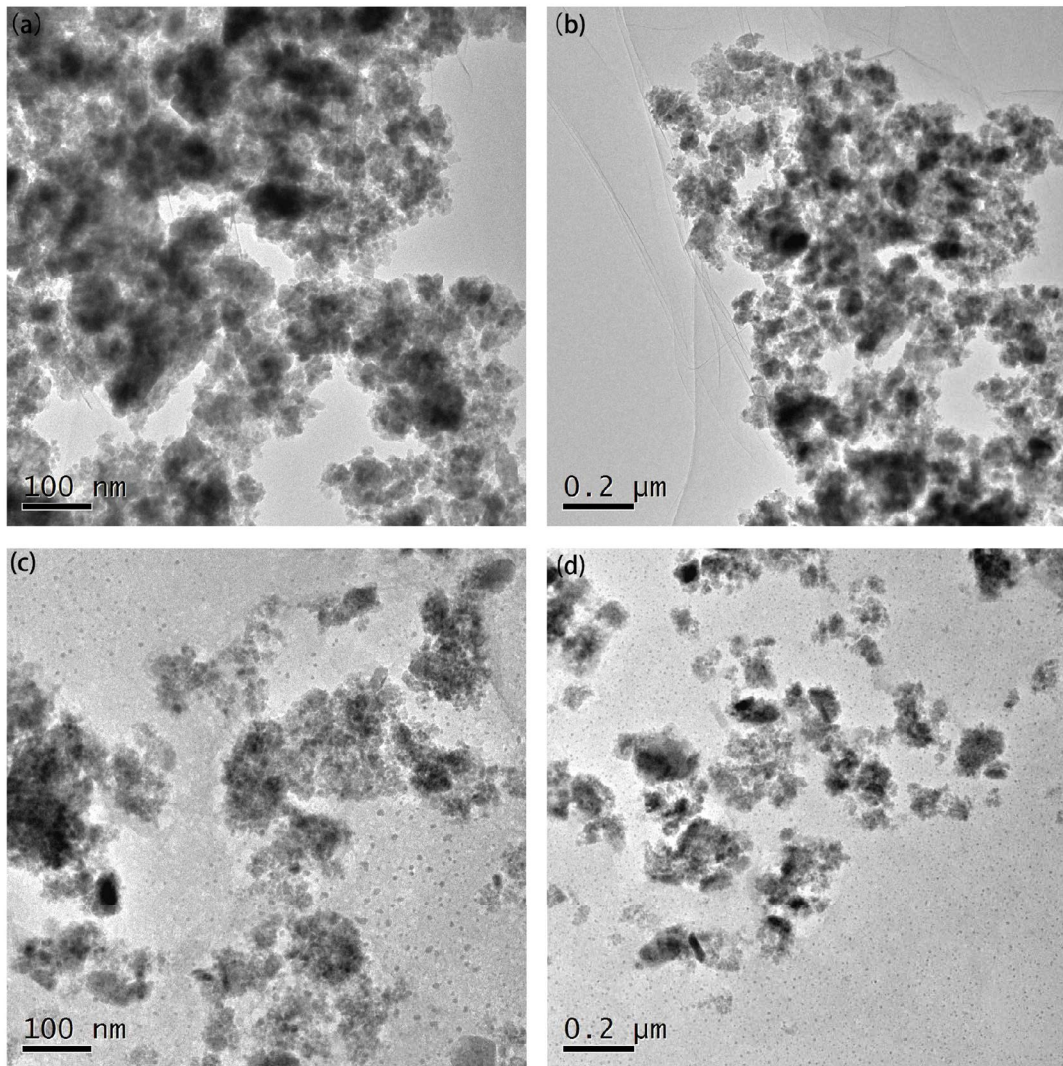


Fig. 2. TEM images of VTM (a and b) and VTM-HA (c and d).

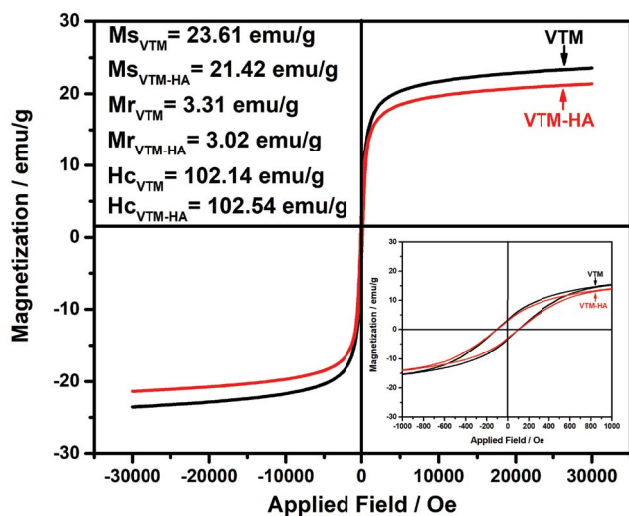


Fig. 3. Magnetization hysteresis loops of the VTM and VTM-HA adsorbent.

the VTM-HA adsorbent is an excellent magnetic material that can be recycled rapidly by magnetic separation.

3.2. Effect of pH

pH value is an important factor of the solution chemical environment. For Zn(II) and Cd(II) ions, their forms would change in the various pH solutions. Besides, the pH values could also affected the chemical state of the VTM-HA adsorbent in the solutions. The adsorption characteristics of Zn(II) and Cd(II) under the pH range of 3–8 were investigated in the single and binary ions solution.

As shown in Fig. 4, the adsorption of Zn(II) and Cd(II) rose rapidly with the growth of pH value from 3 to 6. Then, the growth of adsorption of Zn(II)/Cd(II) almost stopped at the pH range of 7–8, manifesting that the adsorption of Zn(II)/Cd(II) on the VTM-HA adsorbent had achieved equilibration.

Fig. 5 depicts that the competitive effect between Zn(II) and Cd(II) in the binary system made the adsorption capacity of VTM-HA for these two ions decline compared

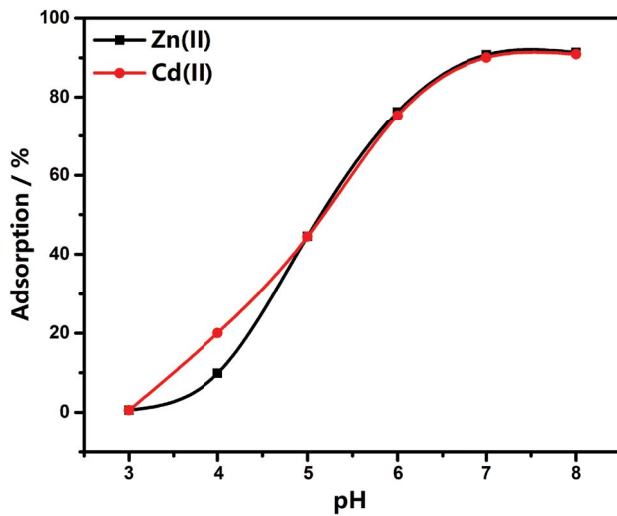


Fig. 4. Effect of pH on the adsorption of Zn(II) and Cd(II) onto VTM-HA in the single ion solution (initial concentration 10 mg/L; VTM-HA 0.4 g/L; contact time 24 h; adsorption temperature 298 K).

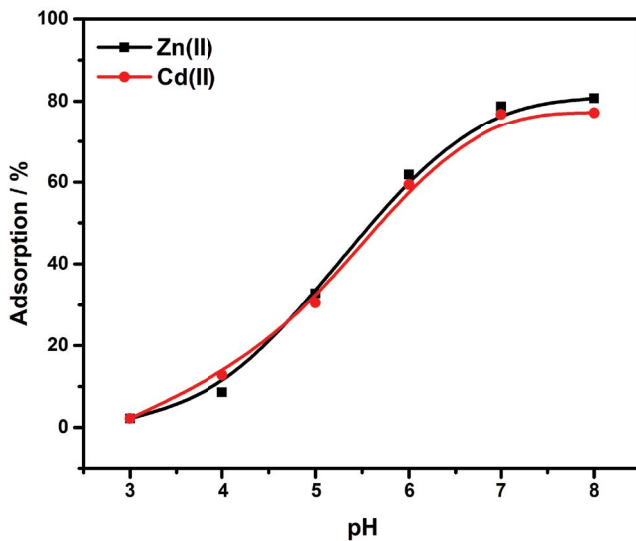


Fig. 5. Effect of pH on the adsorption of Zn(II) and Cd(II) onto VTM-HA in the binary ions solution (initial concentration 10 mg/L; VTM-HA 0.4 g/L; contact time 24 h; adsorption temperature 298 K).

to the single system. The main reason is that there was a competition between Zn(II) and Cd(II) to occupy the adsorbing sites on the VTM-HA adsorbent. In an acidic solution, the H^+ ions would occupy the active sites of the VTM-HA adsorbent, which would make the Zn(II) and Cd(II) releasing from the VTM-HA adsorbent. In addition, the HA molecular would become curly in acidic solution [40]. The number of active sites of VTM-HA decreased because of the crimping of HA, which reduced the adsorption capacity of Zn(II) and Cd(II) on the VTM-HA adsorbent. Based on the above research, the recommended adsorption pH condition ranges from 7 to 8.

3.3. Adsorption kinetics

In this part, two kinetic models, the pseudo-first-order and pseudo-second-order models were used to describe the adsorption kinetic characteristics of Zn(II) and Cd(II). As shown in Fig. 4, the adsorption of Zn(II) and Cd(II) rose rapidly with a pH value of 3–6. Then, the growth of adsorption of Zn(II)/Cd(II) almost stopped at the pH range of 7–8, manifesting that the adsorption of Zn(II)/Cd(II) onto the VTM-HA adsorbent had achieved equilibrium. So, the adsorption kinetics experiments were conducted under pH = 7. The linear form of the equation representing this model are as follows [41,42]:

$$\ln(q_e - q_t) = \ln q_e - k_1 t \quad (2)$$

$$\frac{t}{q_t} = \frac{1}{k_2 q_e^2} + \left(\frac{1}{q_e}\right)t \quad (3)$$

where q_e and q_t (mg/g) are the adsorption amount of Zn(II)/Cd(II) at equilibrium and at a certain time t , respectively. k_1 (min^{-1}) is the rate constant of pseudo-first-order adsorption, and k_2 ($\text{g/mg}\cdot\text{min}$) is the pseudo-second-order rate constant of adsorption.

The curves displayed in Fig. 6a demonstrate the adsorption capacities of Zn(II) and Cd(II) on the VTM-HA increased rapidly with the increase of adsorption time. The adsorption of Zn(II) and Cd(II) on the VTM-HA could achieve equilibrium within 100 min. Extending the adsorption time could hardly increase the adsorbing capacity of Zn(II) and Cd(II) on the VTM-HA adsorbent.

The data exhibited in Figs. 6b and c and Table 1 for each metal ions show a good correspondence with the pseudo-second-order kinetic model, the correlation coefficient R^2 were both higher than 0.99. Therefore, the adsorption of Zn(II) and Cd(II) belonged to chemisorption [43].

3.4. Isothermal adsorption models

3.4.1. Single ion system

Next, the isothermal adsorption method was used to investigate the competitive adsorption between Zn(II) and Cd(II). The isothermal adsorption experiments were, respectively, conducted in a single and binary ions system. In competitive adsorption experiments, the target ion (Zn(II) or Cd(II)) concentrations were controlled at 5–40 mg/L. Meanwhile, the concentration ratio of the target ion to the competing ion was set as 1:0.5, 1:1, and 1:2. The adsorption tests data were analyzed by the Langmuir and Freundlich model listing below [44]:

$$\frac{C_e}{q_e} = \frac{C_e}{q_m} + \frac{1}{(k_L q_m)} \quad (4)$$

$$\log q_e = \log k_F + \left(\frac{1}{n}\right) \log C_e \quad (5)$$

where C_e (mg/L) is the equilibrium concentration of Zn(II) and Cd(II), q_e (mg/g) is the equilibrium adsorption capacity,

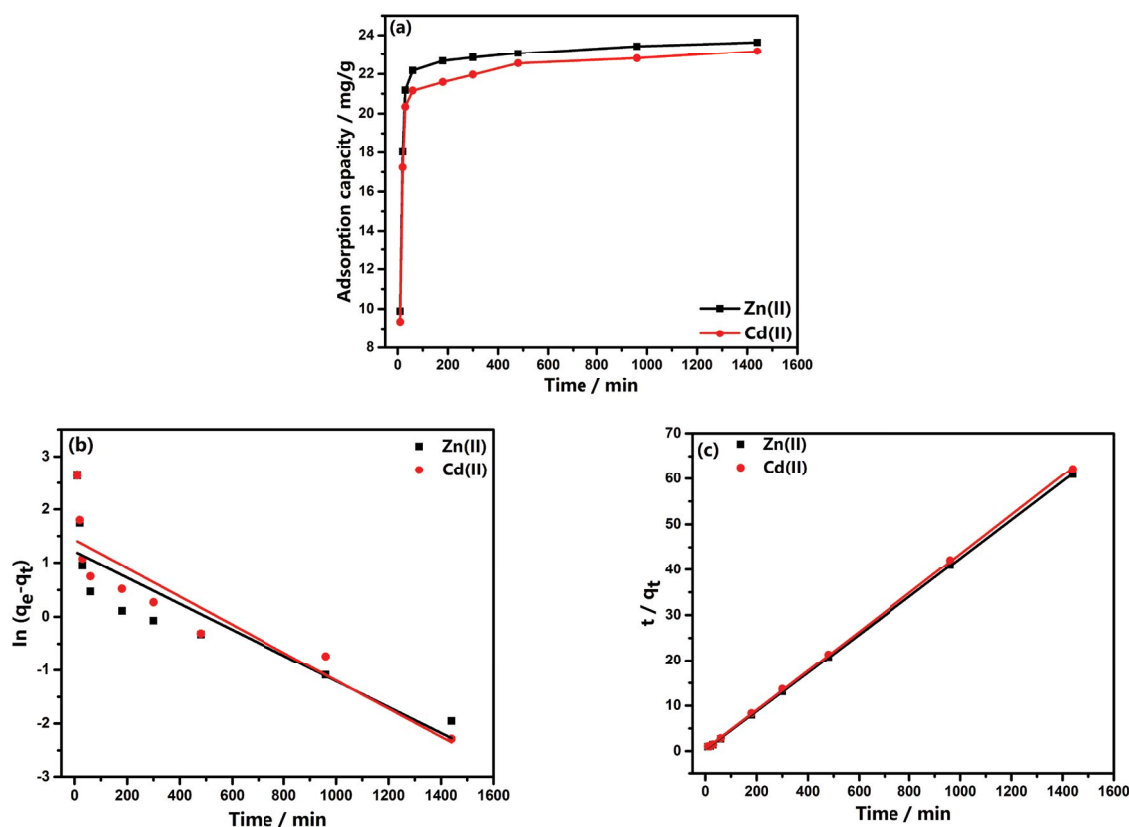


Fig. 6. Adsorbing kinetics fitting of Zn(II)/Cd(II) on the VTM-HA adsorbents. Adsorption amount of Zn(II)/Cd(II) at various time (a), fitting line of the pseudo-first-order model (b), and fitting line of the pseudo-second-order model (c).

Table 1
Parameters of the pseudo-first-order and pseudo-second-order fitting models

Adsorbate	q_e (mg/g)	First-order equation			Pseudo-second-order equation		
		$q_{e,c}$ (mg/g)	k_1 (min ⁻¹)	R^2	$q_{e,c}$ (mg/g)	k_2 (g/mg min)	R^2
Zn(II)	23.775	3.3519	0.00242	0.7194	23.7142	0.004878	0.9999
Cd(II)	23.275	4.1716	0.00262	0.8115	23.2342	0.003875	0.9998

q_m (mg/g) is the maximal adsorption capacity, k_L (L/mg) and k_F (mg¹⁻ⁿ Lⁿ/g) are constants.

Fig. 7 is the linear fitting of the Langmuir and Freundlich model in the single ion system. The fitting data shown in Table 2 revealed that the adsorption quantity of Zn(II) on VTM-HA is more than that of Cd(II). The results could speculate that the adsorbing sites on the VTM-HA for Zn(II) are more than that for Cd(II). The fitting data of Table 2 demonstrate that the correlation coefficients (R^2) of the Langmuir model are higher than that of the Freundlich model, the adsorption of Zn(II) and Cd(II) was more suitable to be described as monolayer adsorption [45].

3.4.2. Binary ions system

Next, the adsorption equilibrium studies were conducted in a binary ions system to investigate the competitive

adsorption. Compared to the single system, the adsorption capacity of VTM-HA adsorbent for one ion (Zn(II) or Cd(II)) in binary solution was obviously suppressed in the presence of the competing ion. The curves of Figs. 8a and b indicate that the adsorption capacity (q_m) of Zn(II) declined with the growth of Cd(II) addition. Similarly, Zn(II) also brought negative effects on the Cd(II) adsorption. There are interference and competition between Zn(II) and Cd(II) for the active adsorption sites in the binary system. The correlation coefficient (R^2) of isothermal models indicated that the adsorption process of Zn(II) and Cd(II) in the binary system both conformed to the Langmuir model, manifesting that the adsorption of Zn(II) and Cd(II) in the binary system also belongs to the chemical adsorption. In addition, the results shown in Table 3 indicate that the addition of Zn(II) has a greater negative effect on Cd(II) adsorption than that of the Cd(II) on Zn(II) adsorption. This result

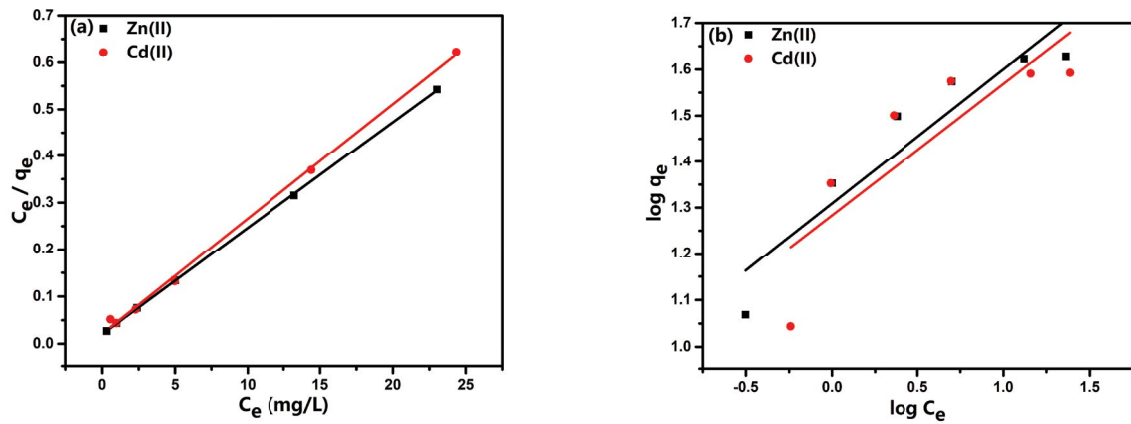


Fig. 7. Langmuir (a) and Freundlich (b) fitting lines for the Zn(II)/Cd(II) adsorption in single solution.

Table 2
Parameters of Langmuir and Freundlich models for Zn(II)/Cd(II) adsorption

Metal ions	Langmuir			Freundlich		
	q_m (mg/g)	k_L (L/mg)	R^2	k_F ($\text{mg}^{1-n} \cdot \text{L}^n/\text{g}$)	$1/n$	R^2
Zn(II)	44.2870	1.1031	0.9998	20.3643	0.2912	0.8553
Cd(II)	40.8664	1.1526	0.9979	19.1818	0.2858	0.6562

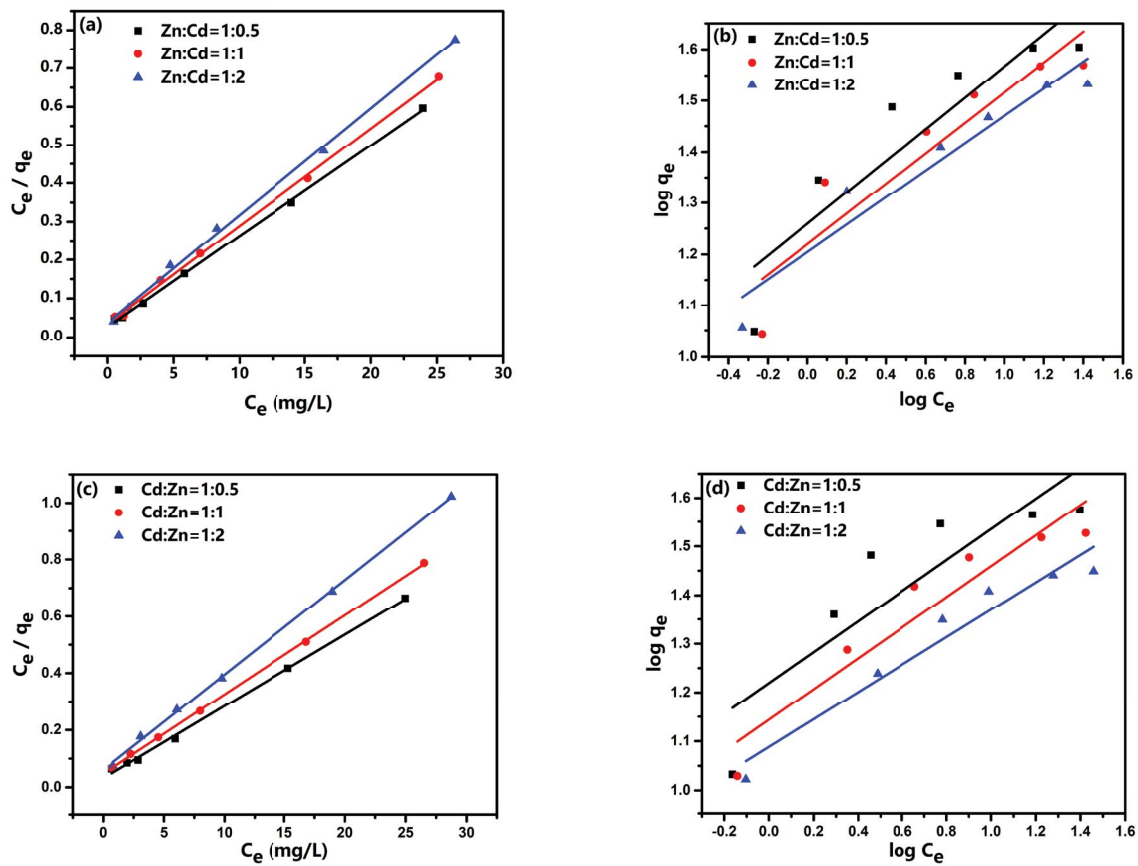


Fig. 8. Langmuir (a and c) and Freundlich (b and d) fitting lines for the Zn(II)/Cd(II) adsorption in various concentration ratio binary solution.

Table 3
Parameters of Langmuir and Freundlich models for Zn(II)/Cd(II) adsorption

Metal ions proportion	Langmuir			Freundlich		
	q_m (mg/g)	k_L (L/mg)	R^2	k_f (mg ¹⁻ⁿ ·L ⁿ /g)	1/n	R^2
Zn:Cd = 1:0.5	42.43	0.8688	0.9992	18.1681	0.3080	0.7831
Zn:Cd = 1:1	39.37	0.7259	0.9987	16.5894	0.2958	0.8237
Zn:Cd = 1:2	35.88	0.7292	0.9979	16.0159	0.2657	0.9116
Cd:Zn = 1:0.5	39.70	0.7934	0.9979	16.5730	0.3159	0.7151
Cd:Zn = 1:1	36.04	0.5786	0.9998	13.9219	0.3157	0.8818
Cd:Zn = 1:2	30.02	0.5401	0.9991	12.2574	0.2814	0.9317

manifested that the Zn(II) ion was dominant in competitive adsorption.

3.4.3. Competitive adsorption model

The above investigation mainly focused on the adsorbing characteristics of a single ion (Zn(II) or Cd(II)) in single or binary ion systems. As we knew, there would be competitive adsorption in a multi-ion system. In order to further research the competitive adsorption characteristics of Zn(II) and Cd(II), the non-modified Langmuir, modified Langmuir, and extended Langmuir models [46,47] were introduced in this study. The model equations could be expressed as follows:

Non-modified Langmuir:

$$q_i = \frac{q_{im} K_i C_i}{1 + \sum_{j=1}^n K_j C_j} \tag{6}$$

Modified Langmuir model:

$$q_i = \frac{q_{im} K_i (C_i \rho_{ii})}{1 + \sum_{j=1}^n K_j C_j \rho_{ij}} \tag{7}$$

where q_{im} (mg/g) is the maximum adsorbing capacity of i ion in single ion system; K_i (L/mg) is the constant of i ion in Langmuir model; C_i (mg/L) is the equilibrium concentration of i ion in multi-ion system; ρ_i is the interaction factor of i ion in the multi-ion system.

Extended Langmuir model:

$$q_i = \frac{Q_{im} K_{ELi} C_i}{1 + \sum_{j=1}^n K_{ELj} C_j} \tag{8}$$

where Q_{im} (mg/g) is the maximum adsorbing capacity of i ion in the multi-ion system; K_{ELi} (L/mg) is the interaction parameter of i ion obtained by extended Langmuir model fitting; C_i (mg/L) is the equilibrium concentration of i ion in the multi-ion system.

Next, the adsorption data of the Zn–Cd binary ion system were analyzed by the mentioned three models using

the least square method and to find which model is the best to describe the competitive adsorption characteristics of Zn(II) and Cd(II). The concentration range of the target ion was controlled from 5 to 40 mg/L, the concentration of the competing ion was set to 10, 20, 30, and 40 mg/L. The fitting parameters are posted in Table 4. The fitting surfaces are displayed in Fig. 9.

It can be seen from Table 4 that the model of extended Langmuir is the most suitable to describe the competitive adsorption between Zn(II) and Cd(II) among these three models. The competition factor ρ_i represents the mutual inhibition of each metal ion in the competitive adsorption process. The larger the competition factor, the more dominant the ion in the competitive adsorption process. It can be seen from Table 4 that the competition factor of Zn(II) ρ_{Zn} is 0.701 and the competition factor of Cd(II) ρ_{Cd} is 0.542, indicating in the Zn(II)/Cd(II) binary system, the adsorption of Zn(II) on the VTM-HA surface is more dominant. The presence of Zn(II) in the solution has a strong inhibitory effect on the adsorption of Cd(II).

3.5. Regenerative ability of VTM-HA

3.5.1. Effect of pH

The previous research indicated that the H⁺ ions would occupy the adsorbing sites of VTM-HA adsorbent, replacing the Zn(II) and Cd(II) ions [48]. That's why the concentration of H⁺ would significantly influence the desorption process of Zn(II) and Cd(II) from the VTM-HA-Zn(II)/Cd(II) complex. The effects of pH value on desorption of Zn(II) and Cd(II) are displayed in Fig. 10.

Table 4
Fitting parameters of competitive adsorption of Zn(II) and Cd(II)

Isothermal models	Parameters	R^2
Non-modified Langmuir	/	0.0235/0.0417
Modified Langmuir	$\rho_{Zn} = 0.701$ $\rho_{Cd} = 0.542$	0.973 0.954
Extended Langmuir	$q_{m-Zn} = 41.502$ mg/g $K_{EL-Zn} = 8.48$ $q_{m-Cd} = 37.862$ mg/g $K_{EL-Cd} = 2.494$	0.759 0.658

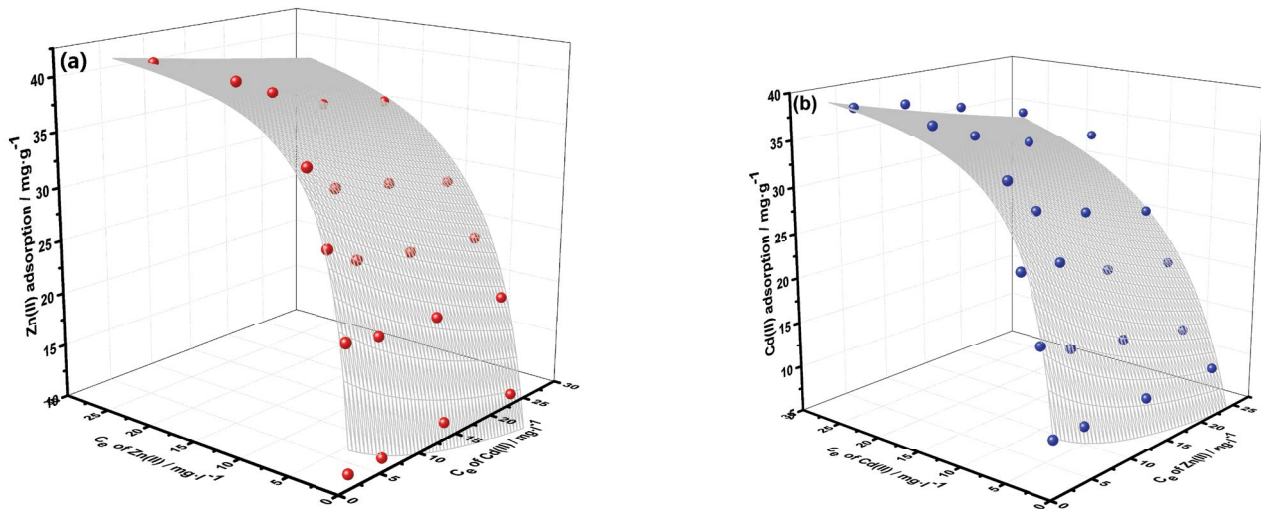


Fig. 9. Fitting surface of Zn(II) and Cd(II) adsorption in the binary system.

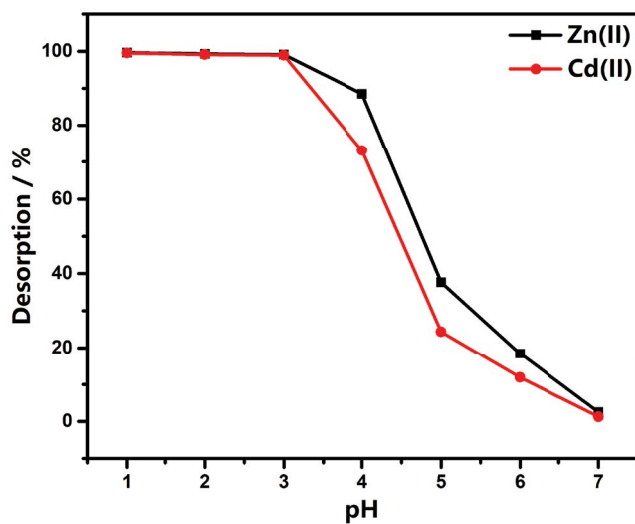


Fig. 10. Desorbing capacity of Zn(II) and Cd(II) at various pH.

As displayed in Fig. 10, the desorption of Zn(II) and Cd(II) maintained at a high level of about 99.6% at pH 1–3. Then the desorption of Zn(II) and Cd(II) sharply declined with the continuous increase of pH value. The main reason is that when the H^+ concentration of solutions drops to a low level, the amount of H^+ ions is not enough to replace the Zn(II) and Cd(II) ions. This result indicated that the Zn(II) and Cd(II) would be adsorbed firmly on the VTM-HA adsorbent in a weakly acidic or neutral solution. The pH range of 1–3 would be suggested to the Zn(II) and Cd(II) desorption process.

3.5.2. Eluent dosage

The eluent dosage is an important influence factor to desorption operation. In this research, the effects of eluent dosage on Zn(II) and Cd(II) desorption by changing

the solid-to-liquid ratio (S/L), which came from the ratio of VTM-HA-Zn(II)/Cd(II) complex amount (g) to the elution solution (L). The volume of the eluant (0.01 M HCl, pH = 2) was controlled at 50 mL. The S/L value was changed from 0.2 to 4.0 g/L.

As shown in Fig. 11, under the various experimental conditions, more than 99.0% of Zn(II) could be desorbed from the VTM-HA-Zn(II)/Cd(II) complex. The desorbing efficiency of Cd(II) was slightly lower than that of Zn(II). Under the condition of S/L = 4.0 g/L, the desorption of Cd(II) also could maintain at about 95%. The results showed that the value of S/L could hardly affect the desorbing efficiency of Zn(II) and Cd(II). Within the experimentally designed S/L range, the desorbing efficiency of Zn(II) and Cd(II) was always maintained at a high level. This result manifested that in desorbing process, the consumption of eluent will be very small.

3.5.3. Regenerative ability

For a novel adsorbent, the regenerative ability should be prioritized. In this research part, the new VTM-HA adsorbent would first be used to adsorb the Zn(II) and Cd(II). Subsequently, the VTM-HA-Zn(II)/Cd(II) complex was put into the eluent with pH = 2. After the desorbing process, the VTM-HA with Zn(II) and Cd(II) dislodged was used again to adsorb the Zn(II) and Cd(II). In order to verify the regenerative ability of VTM-HA adsorbent, five adsorption–desorption cycles were conducted.

Fig. 12 demonstrates that the adsorbing ability of regenerated VTM-HA to Zn(II) and Cd(II) declined about 5% after five adsorption–desorption cycles. The above research results manifested that the VTM-HA adsorbent could still maintain a good adsorbing capacity after many times using. Table 5 lists the regenerative ability of some other adsorbents reported in previously published papers. From the data given in Table 5, we can see that the VTM-HA adsorbent has an excellent regenerative ability comparing with other adsorbents.

Table 5
Comparison of the regenerative capacity of other adsorbents

Adsorbents	Metal ions	Eluent	Cycles	Retained adsorption capacity (%)	Ref.
VTM-HA	Zn(II)/Cd(II)	0.01 M HCl	5	94.40/94.32	This study
Fe ₃ O ₄ @SiO ₂ -NH ₂	Zn(II)	1 M HCl	5	83.3	[49]
MNPs-L	Zn(II)/Cd(II)	6 M HCl	5	86	[50]
CSTU	Zn(II)/Cd(II)	EDTA	5	88.6/85.8	[3]
POPDA/HZO	Cd(II)	0.2 M NaOH	10	95.23	[51]
MWCNTs	Cd(II)	0.1 M HCl	3	92	[52]

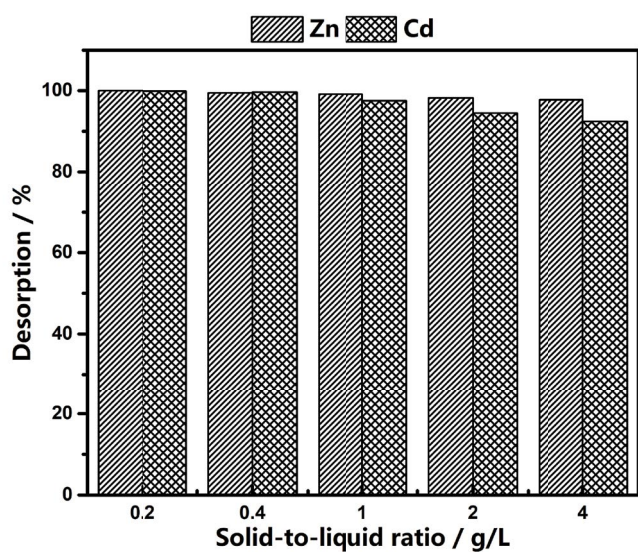


Fig. 11. Desorbing capacity of Zn(II) and Cd(II) under different eluent dosage.

3.6. Zn(II) and Cd(II) adsorption mechanisms

3.6.1. FTIR spectra analyses

The main active component of the VTM-HA is the HA, and the pure HA was used for infrared spectroscopy tests to analyze the functional groups of HA, HA-Zn(II) and HA-Cd(II). The FTIR spectra of HA, HA-Zn(II), and HA-Cd(II) complexes (pH = 7) are displayed in Fig. 13.

The FTIR spectra shown in Fig. 13 reveal that the characteristic peaks of HA after adsorbing Zn(II) and Cd(II) were mainly at 3,000–4,000 cm⁻¹ and 1,000–2,000 cm⁻¹, which belonged to the fingerprint region of hydroxyl and carboxyl [48]. In the original HA spectrum, the peaks at 1,710 and 1,594 cm⁻¹ belonged to the stretching vibration of C=O. The peak at 1,240 cm⁻¹ mainly attached to the stretching vibration of C–O. The signal peak of O–H in carboxyl is at 2,594 cm⁻¹. The peaks at 3,577 and 3,399 cm⁻¹ belonged to O–H of intermolecular hydrogen bonding. After adsorbing metal ions, some FTIR peaks of HA-Zn(II) and HA-Cd(II) complex changed. The dual peaks at 1,568 and 1,370 cm⁻¹ attributed to carboxylate appeared. The peak at 3,073 cm⁻¹ belonged to the intramolecular hydrogen bond of chelate emerged after the Zn(II)/Cd(II) adsorption [53]. It could be speculated that there are some complexation reactions

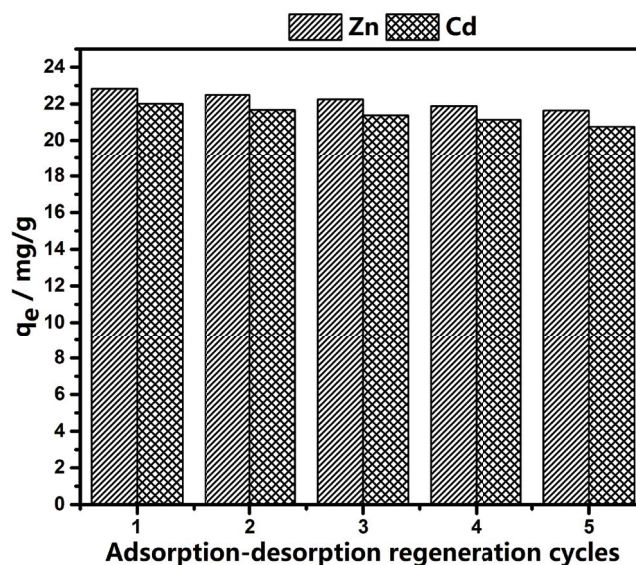


Fig. 12. Adsorbing capacity of the VTM-HA in each regenerative cycle.

between Zn(II)/Cd(II) ions and VTM-HA adsorbent from the FTIR spectra.

3.6.2. XPS analyses

XPS test is a powerful tool to further explore the chemical state of the VTM-HA-Zn(II) and VTM-HA-Cd(II) complexes. The full-scanning XPS spectra are exhibited in Fig. 14a. The narrow-scanning XPS spectra were also conducted to further investigate the chemical state changing of each element during the adsorbing process. The XPS analyses of O1s, Zn2p, and Cd3d are posted in Figs. 14b and c.

As shown in Fig. 14b, the peak of O1s can be divided into five individual peaks: C–O (533 eV), C=O (531.2 eV), O–H (532.1 eV), Fe–O (529.8 eV), and Zn/Cd–O (529.9/529.1 eV) [54]. The intensity of peaks shown in Fig. 14b manifest that the C–O and C=O groups were dominant in the O1s orbit of VTM-HA. The results of Fig. 14c exhibit that the XPS peaks of Zn2p and Cd3d can be divided into two individual peaks: the groups of Zn–O/Cd–O (Zn/Cd–OOC, Zn/Cd–O–C) and Zn/Cd–OH⁺ [55,56]. The Zn2p and Cd3d high-resolution spectra indicated that the Zn(II) and Cd(II) ions were adsorbed by the VTM-HA mainly in the forms of the Zn/

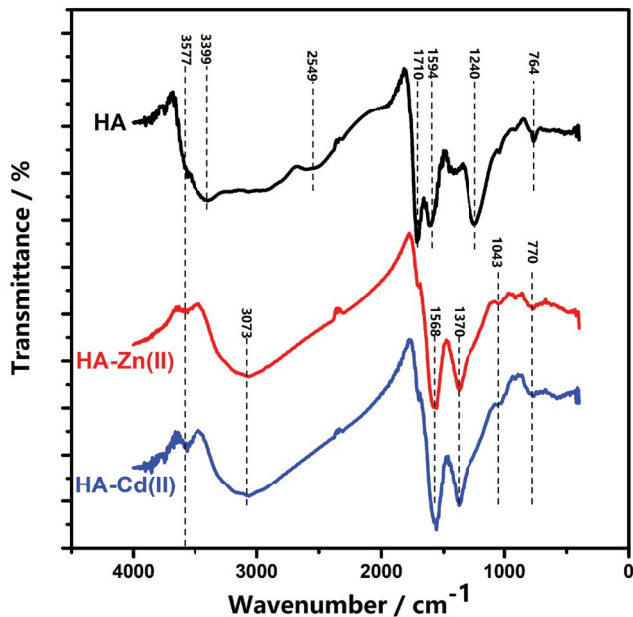


Fig. 13. FTIR spectra of HA-Zn and HA-Cd complex.

Cd-HA complex. A small part of Zn and Cd hydrolyzed in the water, forming Zn/Cd-OH⁺ under the pH = 7.

3.6.3. DFT calculation

In this section, the DFT calculations were used to investigate the binding energy between HA and Zn(II)/Cd(II). However, the structure of the HA is uncertain due to the complexity of HA molecule. Based on the above research results, the primary adsorbing sites in the HA for the heavy metal ions were suggested to be the carboxyl and hydroxyl groups. So, the acetic acid and ethyl alcohol were chosen as the basic ligands to conduct the DFT calculations. As we knew, the frontier molecular orbital theory is the normal method estimating the reaction capacity between two reactors. In this study, the energy gap (ΔE) between the energy of high occupied molecular orbital (E_{HOMO}) and lowest unoccupied molecular orbital (E_{LUMO}) represented the stability of the complex, forming from ligands and Zn(II), Cd(II). The higher the ΔE is, the more stable the molecules are. According to the frontier molecular orbital theory, the DFT calculation gave the ΔE of the complex products formed from acetic acid/ethyl alcohol and Zn(II)/Cd(II). The calculation results are shown in Table 6.

It can be seen from Table 6 that the ΔE of the complex product of acetic acid/ethyl alcohol and Zn(II) is higher than that of the complex product of acetic acid/ethyl alcohol and Cd(II). The results manifest that Zn(II) is more natural to combine with ligands of the HA on the surface of the VTM-HA compared with Cd(II). Also, our previous research results showed that the ΔE between hydrogen ion and hydroxyl/carboxyl is much higher than that between Zn(II)/Cd(II) and hydroxyl/carboxyl [19]. This result manifested that when in the acidic solution, the hydroxyl and carboxyl groups of HA would preferentially bond with hydrogen ions, thus releasing the Zn(II)/Cd(II) ions.

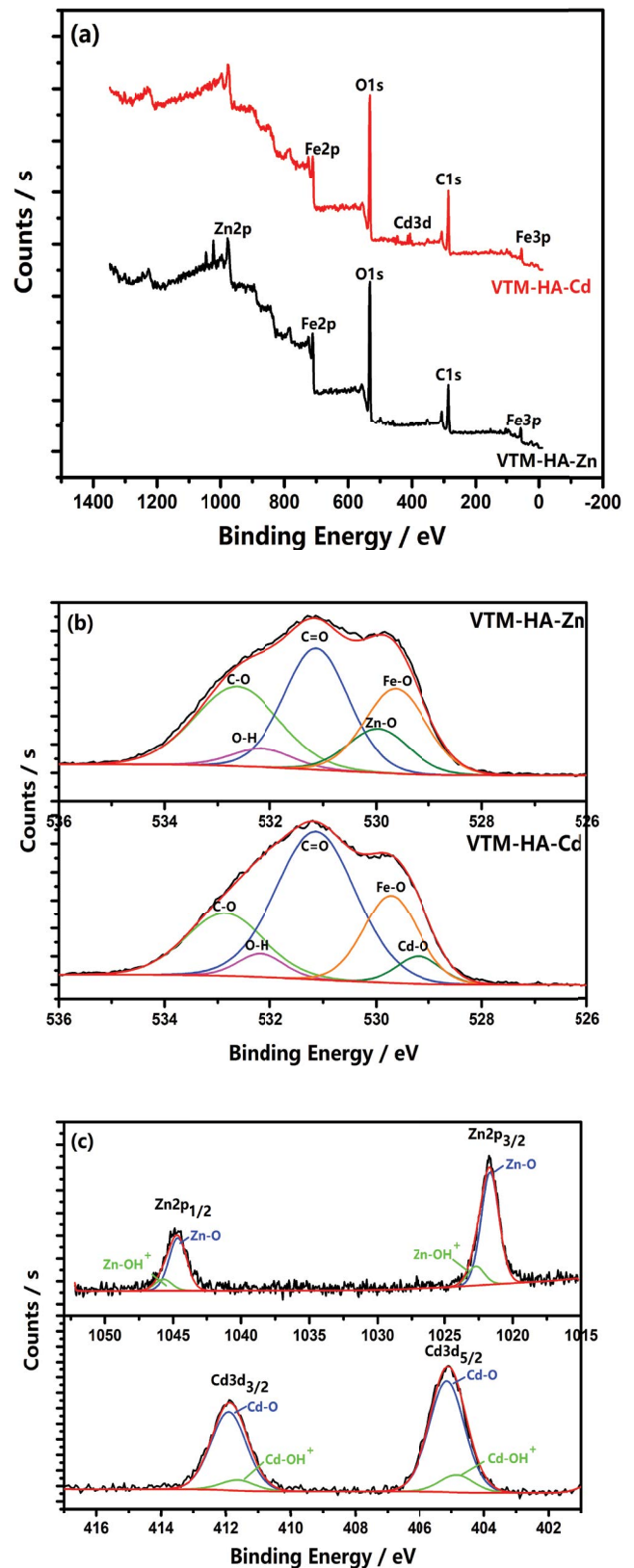
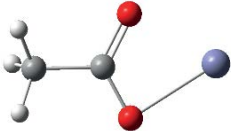
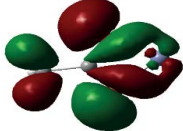

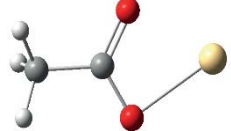
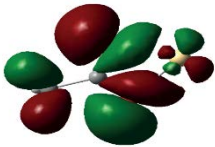
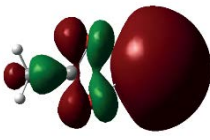
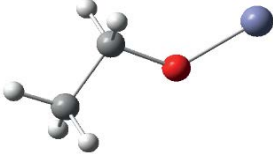
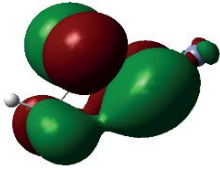
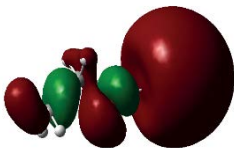
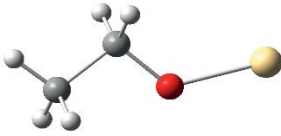
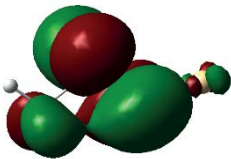
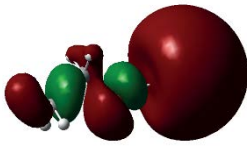


Fig. 14. XPS spectra of VTM-Zn and VTM-Cd (a), the O1s (b), and Zn2p/Cd3d (c) decomposition spectra of VTM-HA-Zn and VTM-HA-Cd complex.

Table 6
Molecular orbital energy of various compounds

Compound species	E_{HOMO} (eV)	E_{LUMO} (eV)	ΔE (eV)
Acetic acid-Zn 	-13.7098 	-10.0639 	3.6459
Acetic acid-Cd 	-13.1245 	-10.0253 	3.0992
Ethyl alcohol-Zn 	-12.7533 	-10.2040 	2.5493
Ethyl alcohol-Cd 	-12.3778 	-9.9907 	2.3871

This is the primary reason that the Zn(II) and Cd(II) adsorbed on the VTM-HA surface could be eluted in the acidic solution.

4. Conclusions

The adsorption experiments showed that the VTM-HA adsorbent is a potential adsorbent for Zn(II) and Cd(II) adsorption. The adsorption kinetics tests indicated that the Zn(II) and Cd(II) adsorption both obey to the pseudo-second-order kinetic model. In the single metal ion system, the maximal adsorbing capacity of Zn(II) and Cd(II) on the VTM-HA adsorbent was 44.29 and 40.87 mg/L, respectively. When in the binary ions solution, the competitive adsorption made the adsorption capacity of VTM-HA for Zn(II) and Cd(II) decline 17.22% and 26.43%, respectively. The competitive adsorption between Zn(II) and Cd(II) could be well-described by the extended Langmuir model. The fitting results demonstrated that the Zn(II) adsorption was dominant in competitive adsorption. The regeneration experiments showed that after five times adsorption-desorption cycles, the VTM-HA still could maintain more than 90% adsorption ability for Zn(II) and Cd(II).

The FTIR and XPS results demonstrated that the Zn(II) and Cd(II) adsorption on the VTM-HA mainly via forming some complexes with the carboxyl and hydroxyl

groups of the HA. The DFT calculation results showed that the ΔE of the complex products of acetic acid/ethyl alcohol and Zn(II) is 3.6459 and 3.0992 eV, respectively, higher than that of the complex products of acetic acid/ethyl alcohol and Cd(II). This manifested that Zn(II) had a higher combining capacity with carboxyl and hydroxyl groups than Cd(II). That is why Zn(II) has an advantage in the competitive adsorption.

Acknowledgments

The authors would express their heartfelt thanks to the National Natural Science Foundation of China (No. U1960114 and 50804059).

References

- [1] Y.H. Zhang, G.X. Cao, Z.B. Zhang, T. Marhaba, Study on removal and stabilization of heavy metals in contaminated sediment using modified clinoptilolite, *Desal. Water Treat.*, 171 (2019) 132–143.
- [2] I. Ounifi, C. Ursino, A. Hafiane, A. Figoli, E. Ferjani, Preparation of thin film composite membranes using interfacial polymerization for treatment of industrial water containing heavy metals, *Desal. Water Treat.*, 170 (2019) 80–90.
- [3] M. Monier, D.A. Abdel-Latif, Preparation of cross-linked magnetic chitosan-phenylthiourea resin for adsorption of Hg(II), Cd(II) and Zn(II) ions from aqueous solutions, *J. Hazard. Mater.*, 209–210 (2012) 240–249.

- [4] T. Sheela, Y.A. Nayaka, R. Viswanatha, S. Basavanna, T.G. Venkatesha, Kinetics and thermodynamics studies on the adsorption of Zn(II), Cd(II) and Hg(II) from aqueous solution using zinc oxide nanoparticles, *Powder Technol.*, 217 (2012) 163–170.
- [5] Z.G. Zheng, H.Y. Zhao, X.H. Lin, J.B. Yang, R.H. Shi, Preparation of activated carbon from *Camellia oleifera* shell and its application to adsorption of hexavalent chromium from aqueous solution: kinetics, equilibrium, and thermodynamics, *Desal. Water Treat.*, 198 (2020) 170–179.
- [6] I.S. Bădescu, D. Bulgariu, I. Ahmad, L. Bulgariu, Valorisation possibilities of exhausted biosorbents loaded with metal ions – a review, *J. Environ. Manage.*, 224 (2018) 288–297.
- [7] A.I.A. Sherlala, A.A.A. Raman, M.M. Bello, A. Asghar, A review of the applications of organo-functionalized magnetic graphene oxide nano composites for heavy metal adsorption, *Chemosphere*, 193 (2019) 1004–1017.
- [8] R.K. Misra, S.K. Jain, P.K. Khatri, Iminodiacetic acid functionalized cation exchange resin for adsorption removal of Cr(VI), Cd(II), Ni(II) and Pb(II) from their aqueous solution, *J. Hazard. Mater.*, 185 (2011) 1508–1512.
- [9] C.M. Xiong, W. Wang, F.T. Tan, F. Luo, J.G. Chen, X.L. Qiao, Investigation on the efficiency and mechanism of Cd(II) and Pb(II) removal from aqueous solution using MgO nanoparticles, *J. Hazard. Mater.*, 299 (2015) 664–674.
- [10] E. Rott, M. Nouri, C. Meyer, R. Minke, M. Schneider, K. Mandel, A. Drenkova-Tuhtan, Removal of phosphonates from synthetic and industrial wastewater with reusable magnetic adsorbent particles, *Water Res.*, 145 (2018) 608–617.
- [11] Q. Du, S.S. Zhang, J.P. Song, Y. Zhao, F. Yang, Activation of porous magnetized biochar by artificial humic acid for effective removal of lead ions, *J. Hazard. Mater.*, 389 (2020), doi: 10.1016/j.jhazmat.2020.122115.
- [12] C.H. Cao, L. Xiao, C.H. Chen, X.W. Shi, Q.H. Cao, L. Gao, *In situ* preparation of magnetic Fe₃O₄/chitosan nanoparticles via a novel reduction-precipitation method and their application in adsorption of reactive azo dye, *Powder Technol.*, 260 (2014) 90–97.
- [13] Z.M. Qiang, X.L. Bao, W.W. Ben, MCM-48 modified magnetic mesoporous nanocomposite as an attractive adsorbent for the removal of sulfamethazine from water, *Water Res.*, 47 (2013) 4107–4114.
- [14] S. Naeimi, H. Faghihian, Performance of novel adsorbent prepared by magnetic metal-organic framework (MOF) modified by potassium nickel hexacyanofreeate for removal of Cs⁺ from aqueous solution, *Sep. Purif. Technol.*, 175 (2017) 255–265.
- [15] F.S.A. Khan, N.M. Mubarak, M. Khalid, R. Walvekar, E.C. Abdullah, S.A. Mazari, S. Nizamuddin, R.R. Karri, Magnetic nanoadsorbents' potential route for heavy metals removal – a review, *Environ. Sci. Pollut. Res.*, 27 (2020) 24342–24356.
- [16] P.G. Jamkhande, N.W. Ghule, A.H. Bamer, M.G. Kalaskar, Metal nanoparticles synthesis: an overview on the methods of preparation, advantages and disadvantages, and applications, *J. Drug Delivery Sci. Technol.*, 53 (2019), doi: 10.1016/j.jddst.2019.101174.
- [17] H.Y. Fu, H.F. He, R.L. Zhu, L. Ling, W.X. Zhang, Q.Z. Chen, Phosphate modified magnetite@ferrihydrite as an magnetic adsorbent for Cd(II) removal from water, soil, and sediment, *Sci. Total Environ.*, 764 (2020), doi: 10.1016/j.scitotenv.2020.142846.
- [18] P. Lu, T.H. Chen, H.B. Liu, P. Li, S.C. Peng, Y. Yang, Green preparation of nanoporous pyrrhotite by thermal treatment of pyrite as an effective Hg(II) adsorbent: performance and mechanism, *Minerals*, 9 (2019), doi: 10.3390/min9020074.
- [19] M.M. Lu, Y.B. Zhang, Y.L. Zhou, Z.J. Su, B.B. Liu, G.H. Li, T. Jiang, Adsorption-desorption characteristics and mechanisms of Pb(II) on natural vanadium, titanium-bearing magnetite-humic acid, *Powder Technol.*, 344 (2019) 947–958.
- [20] Y.B. Zhang, M.M. Lu, Y.L. Zhou, Z.J. Su, B.B. Liu, G.H. Li, T. Jiang, Interfacial interaction between humic acid and vanadium, titanium-bearing magnetite (VTM) particles, *Miner. Proc. Extr. Metall. Rev.*, 41 (2020) 75–84.
- [21] H. Sehaqui, L. Schaufellberger, B. Michen, T. Zimmermann, Humic acid desorption from a positively charged nanocellulose surface, *J. Colloid Interface Sci.*, 504 (2017) 500–506.
- [22] Y.L. Zhou, Y.B. Zhang, P. Li, G.H. Li, T. Jiang, Comparative study on the adsorption interactions of humic acid onto natural magnetite, hematite and quartz: effect of initial HA concentration, *Powder Technol.*, 251 (2014) 1–8.
- [23] Y.L. Zhou, Y.B. Zhang, G.H. Li, Y.D. Wu, T. Jiang, A further study on adsorption interaction of humic acid on natural magnetite, hematite and quartz in iron ore pelletizing process: effect of the solution pH value, *Powder Technol.*, 271 (2015) 155–166.
- [24] Y.B. Zhang, M.M. Lu, Z.J. Su, J. Wang, Y.K. Tu, X.J. Chen, C.T. Cao, F.Q. Gu, S. Liu, T. Jiang, Interfacial reaction between humic acid and Ca-montmorillonite: application in the preparation of a novel pellet binder, *Appl. Clay Sci.*, 180 (2019), doi: 10.1016/j.clay.2019.105177.
- [25] B.J. Ni, Q.S. Huang, C. Wang, T.Y. Ni, J. Sun, W. Wei, Competitive adsorption of heavy metals in aqueous solution onto biochar derived from anaerobically digested sludge, *Chemosphere*, 219 (2019) 351–357.
- [26] J.Q. Deng, Y.G. Liu, S.B. Liu, G.M. Zeng, X.F. Tan, B.Y. Huang, X.J. Tang, S.F. Wang, Q. Hua, Z.L. Yan, Competitive adsorption of Pb(II), Cd(II) and Cu(II) onto chitosan-pyromellitic dianhydride modified biochar, *J. Colloid Interface Sci.*, 506 (2017) 355–364.
- [27] J.H. Park, Y.S. Ok, S.H. Kim, J.S. Cho, J.S. Heo, R.D. Delaune, D.C. Seo, Competitive adsorption of heavy metals onto sesame straw biochar in aqueous solutions, *Chemosphere*, 142 (2016) 77–83.
- [28] C.Z. Fan, K. Li, J.X. Li, D.W. Ying, Y.L. Wang, J.P. Jia, Comparative and competitive adsorption of Pb(II) and Cu(II) using tetraethylenepentamine modified chitosan/CoFe₂O₄ particles, *J. Hazard. Mater.*, 326 (2017) 211–220.
- [29] A.G. Liu, R.D. Gonzalez, Modeling adsorption of copper(II), cadmium(II) and lead(II) on purified humic acid, *Langmuir*, 16 (2000) 3902–3909.
- [30] M.M. Lu, Y.B. Zhang, Z.J. Su, Y.K. Tu, J. Wang, S. Liu, J.C. Liu, T. Jiang, The comprehensive investigation on removal mechanism of Cr(VI) by humic acid-Fe(II) system structured on V, Ti-bearing magnetite surface, *Adv. Powder Technol.*, 32 (2021) 37–51.
- [31] Y.L. Zhou, Y.B. Zhang, G.H. Li, T. Jiang, Effect of metal cations on the fluvic acid (FA) adsorption onto natural iron oxide in iron ore pelletizing process, *Powder Technol.*, 302 (2017) 90–99.
- [32] B. Jiang, Y.F. Gong, J.N. Gao, T. Sun, Y.J. Liu, N. Oturan, M.A. Oturan, The reduction of Cr(VI) to Cr(III) mediated by environmentally relevant carboxylic acids: state-of-the-art and perspectives, *J. Hazard. Mater.*, 365 (2019) 205–226.
- [33] Q. Zhu, Y. Wang, M.F. Li, K. Liu, C.Y. Hu, K.L. Yan, G. Sun, D. Wang, Activable carboxylic acid functionalized crystalline nanocellulose/PVA-co-PE composite nanofibrous membrane with enhanced adsorption for heavy metal ions, *Sep. Purif. Technol.*, 186 (2017) 70–77.
- [34] L.H. Abdel-Rahman, N.M. Ismail, M. Ismael, A.M. Abu-Dief, E.A. Ahmed, Synthesis, characterization, DFT calculations and biological studies of Mn(II), Fe(II), Co(II) and Cd(II) complexes based on a tetradentate ONNO donor schiff base ligand, *J. Mol. Struct.*, 1134 (2017) 851–862.
- [35] F.J. Rodríguez, P. Schlenger, M. García-Valverde, Monitoring changes in the structure and properties of humic substances following ozonation using UV-vis, FTIR and ¹H NMR techniques, *Sci. Total Environ.*, 541 (2016) 623–637.
- [36] K. Yang, H.B. Peng, Y.H. Wen, N. Li, Re-examination of characteristic FTIR spectrum of secondary layer in bilayer oleic acid-coated Fe₃O₄ nanoparticles, *Appl. Surf. Sci.*, 256 (2010) 3093–3097.
- [37] Y.A. Chesalov, T.V. Andrushkevich, V.I. Sobolev, G.B. Chernobay, FTIR study of β-picoline and pyridine-3-carbaldehyde transformation on V-Ti-O catalysts. The effect of sulfate content on β-picoline oxidation into nicotinic acid, *J. Mol. Catal. A: Chem.*, 380 (2013) 118–130.
- [38] H.F. Chen, Q. Li, M.X. Wang, D.B. Ji, W.F. Tan, XPS and two-dimensional FTIR correlation analysis on the binding

- characteristics of humic acid onto kaolinite surface, *Sci. Total Environ.*, 724 (2020), doi: 10.1016/j.scitotenv.2020.138154.
- [39] L.H.S. Vieira, C.M.S. Sabina, F.H.S. Júnior, J.S. Rocha, M.O. Castro, R.S. Alencar, L.S. da Costa, B.C. Viana, A.J. Paula, J.M. Soares, A.G.S. Filho, L. Otubo, P.B.A. Fechine, A. Ghosh, O.P. Ferreira, Strategic design of magnetic carbonaceous nanocomposites and its application as multifunctional adsorbent, *Carbon*, 161 (2020) 758–771.
- [40] M. Zhu, H.T. Wang, A.A. Keller, T. Wang, F.T. Li, The effect of humic acid on the aggregation of titanium dioxide nanoparticles under different pH and ionic strengths, *Sci. Total Environ.*, 487 (2014) 375–380.
- [41] Y.J. Dai, J.J. Li, Q.Y. Sun, Z.H. Liu, Adsorption isotherm, kinetic modeling and mechanism of neutral red on *Auricularia auricularia*, *Desal. Water Treat.*, 198 (2020) 335–344.
- [42] Y.T. Han, X. Cao, X. Ouyang, S.P. Sohi, J.W. Chen, Adsorption kinetics of magnetic biochar derived from peanut hull on removal of Cr(VI) from aqueous solution: effects of production conditions and particle size, *Chemosphere*, 145 (2016) 336–341.
- [43] J.P. Simonin, On the comparison of pseudo-first order and pseudo-second order rate laws in the modeling of adsorption kinetics, *Chem. Eng. J.*, 300 (2016) 254–263.
- [44] S.X. Bai, M. Chu, L.M. Zhou, Z.B. Chang, C. Zhang, H. Guo, B.M. Liu, S.T. Wang, Modified oil shale ash and oil shale ash zeolite for the removal of Cd²⁺ ion from aqueous solutions, *Environ. Technol.*, 40 (2019) 1485–1493.
- [45] M. Naushad, S. Vasudevan, G. Sharma, A. Kumar, Z.A. Allothman, Adsorption kinetics, isotherms, and thermodynamic studies for Hg²⁺ adsorption from aqueous medium using alizarin red-S-loaded amberlite IRA-400 resin, *Desal. Water Treat.*, 57 (2016) 18551–18559.
- [46] L. Leila, R. Cheraghi, R. Dabbagh, G. McKay, Removal of cobalt(II) ions from aqueous solutions utilizing the pre-treated 2-Hypnea Valentiae algae: equilibrium, thermodynamic, and dynamic studies, *Chem. Eng. J.*, 331 (2018) 39–47.
- [47] C.J. Radke, J.M. Prausnitz, Thermodynamics of multi-solute adsorption from dilute liquid solutions, *AIChE J.*, 18 (1972) 761–768.
- [48] Z.F. Ren, X. Xu, X. Wang, B.Y. Gao, Q.Y. Yue, W. Song, L. Zhang, H.T. Wang, FTIR, Raman, and XPS analysis during phosphate, nitrate and Cr(VI) removal by amine cross-linking biosorbent, *J. Colloid Interface Sci.*, 468 (2016) 313–323.
- [49] S.Y. Bao, L.H. Tang, K. Li, P. Ning, J.H. Peng, H.B. Guo, T.T. Zhu, Y. Liu, Highly selective removal of Zn(II) ion from hot-dip galvanizing pickling waste with amino-functionalized Fe₃O₄@SiO₂ magnetic nano-adsorbent, *J. Colloid Interface Sci.*, 462 (2016) 235–242.
- [50] S.Z. Guo, P.P. Jiao, Z.G. Dan, N. Duan, G.Y. Chen, J. Zhang, Preparation of L-arginine modified magnetic adsorbent by one-step method for removal of Zn(II) and Cd(II) from aqueous solution, *Chem. Eng. J.*, 317 (2017) 999–1011.
- [51] N. Rahman, M. Nasir, Application of Box–Behnken design and desirability function in the optimization of Cd(II) removal from aqueous solution using poly(o-phenylenediamine)/hydrous zirconium oxide composite: equilibrium modeling, kinetic and thermodynamic studies, *Environ. Sci. Pollut. Res.*, 25 (2018) 26114–26134.
- [52] M. Alimohammady, M. Jahangiri, F. Kiani, H. Tahermansouri, A new modified MWCNTs with 3-aminopyrazole as a nano-adsorbent for Cd(II) removal from aqueous solutions, *J. Environ. Chem. Eng.*, 5 (2017) 3405–3417.
- [53] X. Zhong, W. Liang, Z.P. Lu, B.W. Hu, Highly efficient enrichment mechanism of U(VI) and Eu(III) by covalent organic frameworks with intramolecular hydrogen-bonding from solutions, *Appl. Surf. Sci.*, 504 (2020), doi: 10.1016/j.apsusc.2019.144403.
- [54] M. Todea, M. Muresan-Pop, S. Simon, C. Moisesescu-Goia, V. Simon, D. Eniu, XPS investigation of new solid forms of 5-fluorouracil with piperazine, *J. Mol. Struct.*, 1165 (2018) 120–125.
- [55] G. Lakshminarayana, S.O. Baki, A. Lira, M.I. Sayyed, I.V. Kityk, M.K. Halimah, M.A. Mahdi, X-ray photoelectron spectroscopy (XPS) and radiation shielding parameters investigations for zinc molybdenum borotellurite glasses containing different network modifiers, *J. Mater. Sci.*, 52 (2017) 7394–7414.
- [56] W.C. Yang, Q.Z. Tang, J.M. Wei, Y.J. Ran, L.Y. Chai, H.Y. Wang, Enhanced removal of Cd(II) and Pb(II) by composites of mesoporous carbon stabilized alumina, *Appl. Surf. Sci.*, 369 (2016) 215–223.